Turkish Journal of Electrical Engineering & Computer Sciences

http://journals.tubitak.gov.tr/elektrik/

Research Article

Turk J Elec Eng & Comp Sci
(2017) 25: 3684 – 3698

doi:10.3906/elk-1605-364

Force and torque parameter estimation for a 4-pole hybrid electromagnet by ANFIS hybrid learning algorithm

Murat ATLIHAN, Barış Can YALÇIN*, Kadir ERKAN
Department of Mechatronics Engineering, Faculty of Mechanical Engineering, Yıldız Technical University, İstanbul, Turkey

Received: 31.05.2016 • **Accepted/Published Online:** 27.05.2017 • **Final Version:** 05.10.2017

Abstract: In this study, a force and torque estimation method based on an adaptive neuro-fuzzy inference system (ANFIS) has been developed to get rid of multiple integral calculations of air gap coefficients that cause time delay for magnetic levitation control applications. During magnetic levitation applications that contain a 4-pole hybrid electromagnet, multiple integral calculations have to be done for obtaining air gap permanence parameters, and these parameters are needed to calculate force and torque parameters that are produced by the poles of the hybrid electromagnet, which means, if time delay occurs for calculation of permanence parameters, actual force and actual torque values that are produced by hybrid electromagnet's poles cannot be exactly known; thus, the advantage of having an exact model of the system gets lost and, as a result, the controller's performance goes down. To address a solution, an ANFIS using a hybrid learning algorithm consisting of backpropagation and least-squares learning methods is proposed to estimate force and torque parameters using training data already obtained using multiple integral calculations before.

Key words: Magnetic levitation, hybrid electromagnet, parameter estimation, ANFIS, learning algorithm

1. Introduction

Applications of magnetic levitation systems have gained expanding importance in industry during the last few decades. The most popular usage areas are magnetic bearings [1–4], transportation systems [5–7], and actuation of objects in micro- and nanoscales [8,9]. Because there is no mechanical contact between levitation system and levitating object, consisting of a ferromagnetic material, mechanical friction has almost no effect on system parameters (except air friction, which has a comparatively low value) on the levitating object [10]. However, there are also some disadvantages, such as the system model is highly nonlinear, and even though some methods may be useful for linearization at some certain points, obtained linear models show unstable system behavior [10,11].

In magnetic levitation systems, conventional u-type electromagnets can only control one degree of freedom; thus, they cannot form a magnetic levitation system that works in several axes. For constructing a u-type electromagnet that has working space including more than one axis, multiple electromagnets have to be located on a plane and be controlled in such a way that every coil of the pole is being energized in some kind of special order. These electromagnets are named 4-pole hybrid electromagnets; each pole consists of both a permanent magnet and a coil. Energizing coils in a different sequence means that controllable moment values exist on the levitated object and the system gains the ability to rotate around the X and Y axes.

*Correspondence: bariscanyalcin@gmail.com

When the coils are fed by current, magnetic flux occurs on electromagnets proportional to applied current and because of the ferromagnetic property of the plane object the poles start generating magnetic force to push or pull the ferromagnetic object. Direction of the magnetic force depends on the direction of the applied current for each pole. The problem here is that, magnetic flux (and of course magnetic force occurring) is not the function of current just by itself; there are also some other parameters that have crucial effects on the value of magnetic flux, such as the magnetic permanence of the air gap between a pole and ferromagnetic plane and also the magnetic permanence of the permanent magnet of the electromagnet. Even though the permanence of the permanent magnet can be assumed as a static value, the magnetic permanence of the air gap depends on translational position along the Z axis and rotational positions around the X and Y axes of a pole for a static ferromagnetic plane. Moreover, the calculation of the magnetic permanence of the air gap contains multiple integrals with nonlinear terms.

Calculation of the magnetic permanence of the air gap for each pole in a small sampling time weakens any control algorithm; the main reason for this situation is that calculation of the magnetic permanence of the air gap for each pole means that applied force by each pole is being obtained, when a time delay occurs in data acquisition because of the low processing speed of the data acquisition card (and it is commonly accepted that every magnetic levitation application requires very high processing data acquisition speed due to magnetic levitation's highly nonlinear nature [12]), proper actuation signals for coils cannot be produced. As an alternative solution, one may think that using a force sensor may be useful; however, many magnetic levitation systems are very vulnerable in terms of disturbance and, because of this, using a force sensor is not a good engineering implementation; in some cases, the electromagnetic force is generally measured by an additional system consisting of a copy of the levitating object located in a load cell [12,13]. The only remaining reasonable technique for success of controlling magnetic levitation systems is estimating the magnetic force value for each pole.

The main contribution of this work is to design a kind of expert system that can be used as a *"look-up table"* for force and torque values produced by hybrid electromagnets in some specific conditions. Almost every magnetic levitation system that is popularly being used in industrial applications and in academic research works under the condition of very fast sampling rates for data acquisition. This fact brings some disadvantages, such as high costs for data acquisition cards and power consumption, if one wants to control the system measuring actual force and actual torque values acting on it. The point is, if a trustworthy estimation method could be developed for estimation of acting force and actual torque values, reduction of computer processing power would be achieved decreasing calculations for obtaining actual acting force and actual torque values applied by poles of hybrid electromagnet. Thus, more complex control algorithms requiring higher energy levels can be used, instead of wasting processor power for calculation of force parameters.

2. 4-Pole hybrid electromagnet structure

A simple 4-pole hybrid electromagnet structure can be seen in Figure 1 below; it has three degrees of freedom, one translational axis Z, and two rotational axes X and Y.

As can be seen in Figure 2, moment values around the Y axis and X axis depend on system design parameters a and b. a represents the distance from the closest edge of each pole to rotation axes, while b represents the distance from the furthest edge of each pole to the center of gravity.

Process of energizing coils can be seen in Figure 3 below. Three virtual winding currents are defined as I_z, I_α, and I_β. These parameters represent a sort of average current working for only one axis (Z, α, or β).

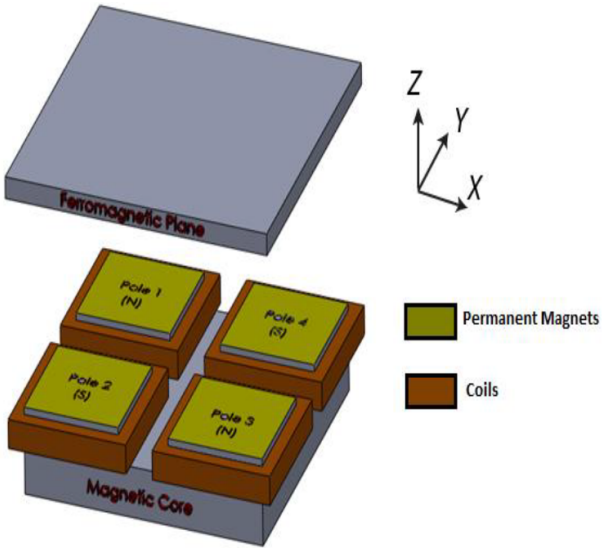

Figure 1. 4-Pole hybrid electromagnet.

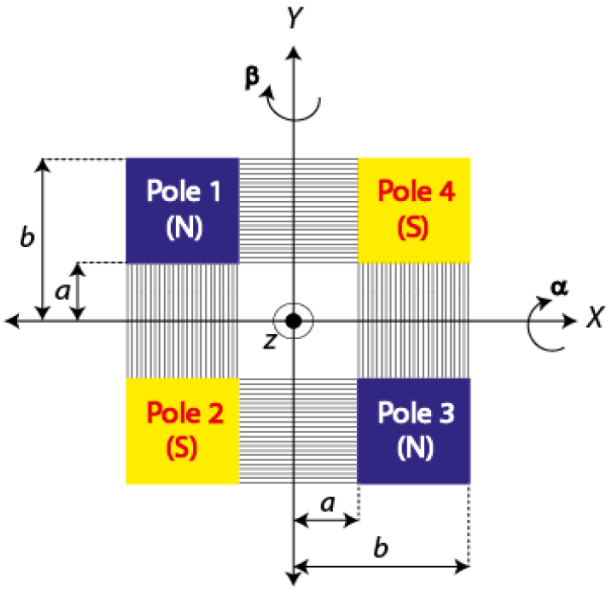

Figure 2. Top view of 4-pole hybrid electromagnet and its axes.

This assumption gives an opportunity for controlling each degree of freedom while controlling I_1, I_2, I_3, and I_4 independently.

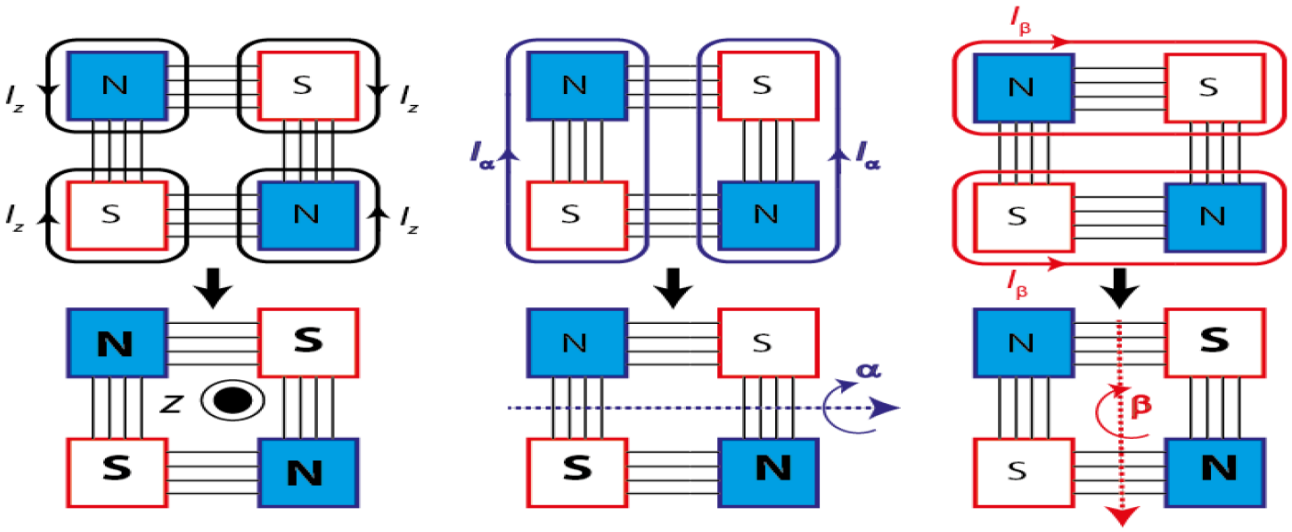

Figure 3. Energizing coils.

Controlling the system for translational movement along the Z axis, I_1, I_2, I_3, and I_4 have to be positive and their average value is calculated in Eq. (1).

Controlling the system for translational movement around the α axis, I_1 and I_4 have to be negative, while I_2 and I_3 have to be positive and their average value is calculated in Eq. (2).

Controlling the system for translational movement around the β axis, I_1 and I_2 have to be negative,

while I_3 and I_4 have to be positive and their average value is calculated in Eq. (3).

$$I_z = \frac{1}{4}\left(I_1 + I_2 + I_3 + I_4\right) \tag{1}$$

$$I_\alpha = \frac{1}{4}(-I_1 + I_2 + I_3 - I_4) \tag{2}$$

$$I_\beta = \frac{1}{4}(-I_1 - I_2 + I_3 + I_4) \tag{3}$$

$$\begin{bmatrix} I_1 \\ I_2 \\ I_3 \\ I_4 \end{bmatrix} = \begin{bmatrix} 1 & -1 & -1 \\ 1 & 1 & -1 \\ 1 & 1 & 1 \\ 1 & -1 & 1 \end{bmatrix} \begin{bmatrix} I_z \\ I_\alpha \\ I_\beta \end{bmatrix} \tag{4}$$

In the second row of Figure 3, it is implied that bold and bigger characters are energized coils; however, the system behaves as if coils are being energized with some virtual winding currents as shown in the first row of Figure 3.

Considering movements of all poles, translational displacement z, along the Z axis, and rotational displacements α and β, around the X and Y axes, respectively, can be written as below.

$$z = \frac{1}{4}\left(z_1 + z_2 + z_3 + z_4\right) \tag{5}$$

$$\alpha = \frac{1}{2b}\left(\frac{z_1 + z_4}{2} - \frac{z_2 + z_3}{2}\right) \tag{6}$$

$$\beta = \frac{1}{2b}\left(\frac{z_1 + z_2}{2} - \frac{z_3 + z_4}{2}\right) \tag{7}$$

In the working principle of hybrid electromagnets, the permanent magnet of each coil behaves as if it is a magnetomotive force source. E_{pm} represents the magnetomotive force source parameter, whereas each coil is a magnetomotive force source, represented as NI; N is number of turns and I is current. The permanence value of each permanent magnet is inversely proportional to the reluctance value of the permanent magnet as shown in Eq. (8) below. R_{pm} represents the reluctance value for each permanent magnet.

$$P_{pm} = \frac{1}{R_{pm}} \tag{8}$$

The air gap between poles and ferromagnetic plane core is also represented as a reluctance parameter, R_{gap}. To identify the relationship between magnetic flux values φ_i produced by poles and magnetomotive force sources (permanent magnets and coils), the equivalent magnetic circuit of the 4-pole electromagnet is shown in Figure 4 below.

The bold arrows around the square in Figure 4 represent the direction of magnetic flux in the circuit.

If the circuit given in Figure 4 is analyzed with respect to the mesh-current method shown in Figure 5, Eqs. (9), (10), (11), (12), (13), (14), (15), and (16) are obtained.

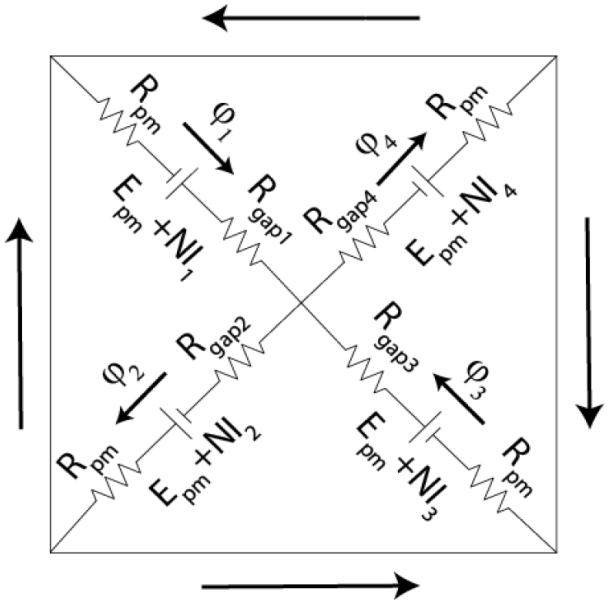

Figure 4. Equivalent magnetic circuit of 4-pole hybrid electromagnet.

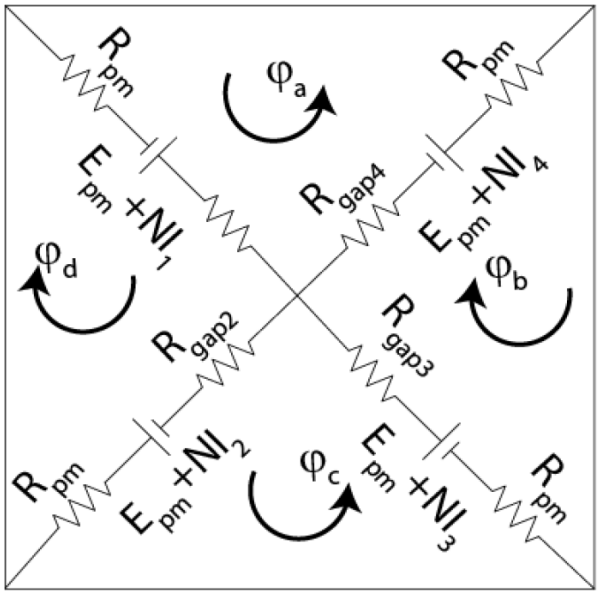

Figure 5. Mesh-current method.

$$\varphi_a R_{gap4} + \varphi_a R_{gap1} + 2\varphi_a R_{pm} - (E_{pm} + NI_4) - (E_{pm} + NI_1) = 0 \tag{9}$$

$$\varphi_b R_{gap4} + \varphi_b R_{gap3} + 2\varphi_b R_{pm} - (E_{pm} + NI_4) - (E_{pm} + NI_3) = 0 \tag{10}$$

$$\varphi_c R_{gap2} + \varphi_c R_{gap3} + 2\varphi_c R_{pm} - (E_{pm} + NI_2) - (E_{pm} + NI_3) = 0 \tag{11}$$

$$\varphi_d R_{gap2} + \varphi_d R_{gap1} + 2\varphi_d R_{pm} - (E_{pm} + NI_2) - (E_{pm} + NI_1) = 0 \tag{12}$$

$$\varphi_1 = \varphi_a + \varphi_d \tag{13}$$

$$\varphi_2 = \varphi_d + \varphi_c \tag{14}$$

$$\varphi_3 = \varphi_b + \varphi_c \tag{15}$$

$$\varphi_4 = \varphi_a + \varphi_b \tag{16}$$

Therefore, magnetic flux parameters produced by each pole can be written as below:

$$\varphi_a = \frac{2E_{pm} + NI_1 + NI_4}{2R_{pm} + R_{gap1} + R_{gap4}} \tag{17}$$

$$\varphi_b = \frac{2E_{pm} + NI_3 + NI_4}{2R_{pm} + R_{Gap3} + R_{Gap4}} \tag{18}$$

$$\varphi_c = \frac{2E_{pm} + NI_2 + NI_3}{2R_{pm} + R_{gap2} + R_{gap3}} \tag{19}$$

$$\varphi_d = \frac{2E_{pm} + NI_1 + NI_2}{2R_{pm} + R_{gap1} + R_{gap2}} \tag{20}$$

$$\varphi_1 = \frac{2E_{pm} + NI_1 + NI_4}{2R_{pm} + R_{gap1} + R_{gap4}} + \frac{2E_{pm} + NI_1 + NI_2}{2R_{pm} + R_{gap1} + R_{gap2}} \tag{21}$$

$$\varphi_2 = \frac{2E_{pm} + NI_1 + NI_2}{2R_{pm} + R_{gap1} + R_{gap2}} + \frac{2E_{pm} + NI_2 + NI_3}{2R_{pm} + R_{gap2} + R_{gap3}} \tag{22}$$

$$\varphi_3 = \frac{2E_{pm} + NI_3 + NI_4}{2R_{pm} + R_{gap3} + R_{gap4}} + \frac{2E_{pm} + NI_2 + NI_3}{2R_{pm} + R_{gap2} + R_{gap3}} \tag{23}$$

$$\varphi_4 = \frac{2E_{pm} + NI_1 + NI_4}{2R_{pm} + R_{gap1} + R_{gap4}} + \frac{2E_{pm} + NI_3 + NI_4}{2R_{pm} + R_{gap3} + R_{gap4}} \tag{24}$$

So far, magnetic flux parameters have been given. Now, the final step before obtaining f_z, T_α, and T_β parameters is to calculate the air gap permanence parameters for each pole. The problem here is, during any magnetic levitation process (including force control, position control, velocity control, or acceleration control), P_{gap} values have to be calculated to determine applied magnetic flux, and applied force and torque parameters are functions of applied magnetic flux. The levitated object's coordinates in the three dimensional space of euclidean geometry, which are parameters of function P_{gap}, dynamically change in time, and calculating these parameters before producing control signal for each coil is hard work for any computer processors. Because of this reason, this process causes a time delay and cost for required high-tech computers. P_{gap} parameters for each coil are given in the equations below.

$$P_{gap1} = \int_a^b \int_{-b}^{-a} \frac{\mu_0}{z - y\tan\beta + x\tan\alpha} dxdy \tag{25}$$

$$P_{gap2} = \int_{-b}^{-a} \int_{-b}^{-a} \frac{\mu_0}{z - y\tan\beta + x\tan\alpha} dxdy \tag{26}$$

$$P_{gap3} = \int_{-b}^{-a} \int_{a}^{b} \frac{\mu_0}{z - y\tan\beta + x\tan\alpha} dxdy \tag{27}$$

$$P_{gap4} = \int_{a}^{b} \int_{a}^{b} \frac{\mu_0}{z - y\tan\beta + x\tan\alpha} dxdy \tag{28}$$

After calculating P_{gap} values, magnetic flux values for each pole can be calculated. In Eq. (29) below, magnetic field density value B_i is obtained using magnetic flux value φ_i for each pole. S is pole surface area.

$$B_i = \frac{\varphi_i}{S} \ , \ \ i = 1, 2, 3, 4 \tag{29}$$

Force value produced by a single pole is given in Eq. (30) below. μ_0 is the permeability constant.

$$f_i = \frac{B_i^2 S}{2\mu_0} \ , \ \ i = 1,2,3,4 \tag{30}$$

After obtaining force values for each pole, finally the total force on the Z axis, f_z value, can be calculated as shown in Eq. (31):

$$f_z = f_1 + f_2 + f_3 + f_4 \tag{31}$$

Additionally, torque values for the X and Y axes can be calculated as follows:

$$T_\alpha = (f_1 - f_2 - f_3 + f_4)\left(\frac{b-a}{2} + a\right) \tag{32}$$

$$T_\beta = (f_1 + f_2 - f_3 - f_4)\left(\frac{b-a}{2} + a\right) \tag{33}$$

For each sampling time, finding analytical solutions of Eqs. (25), (26), (27), and (28) is of crucial importance for obtaining f_z, T_α, and T_β values given in Eqs. (31), (32), and (33), respectively.

The physical parameters used in this study are given in the Table below.

Table. Physical parameters.

Parameter	a [m]	b [m]	μ_0	R_{pm}	S[m^2]	N	E_{pm}
Value	0.0450	0.0810	1.256×10^{-6}	7.9577×10^5	0.0031	200	3115

3. ANFIS structure

As mentioned in the introduction section, α, β, z, I_1, I_2, I_3, and I_4 parameters are used as the training process inputs in the ANFIS hybrid learning algorithm. Three membership functions (MFs) are used for each input, and there are three consequent functions overall (consequent functions consist of consequent parameters and are updated based on least-squares learning algorithm). The ANFIS model structure can be seen in Figure 6 below.

3.1. Layers

In Layer-1, $O_{l,i}$ is the output of the i_{th} node of the layer l. Every node i in this layer is an adaptive node with a node function as follows:

$$O_{1,i} = \mu_{A_i}(x) \ \text{ for } \ i = 1,2,3 \tag{34}$$

$$O_{1,i} = \mu_{B_{i-3}}(x) \ \text{ for } \ i = 4,5,6 \tag{35}$$

$$O_{1,i} = \mu_{C_{i-6}}(x) \ \text{ for } \ i = 7,8,9 \tag{36}$$

$$O_{1,i} = \mu_{D_{i-9}}(x) \ \text{ for } \ i = 10,11,12 \tag{37}$$

$$O_{1,i} = \mu_{E_{i-12}}(x) \ \text{ for } \ i = 13,14,15 \tag{38}$$

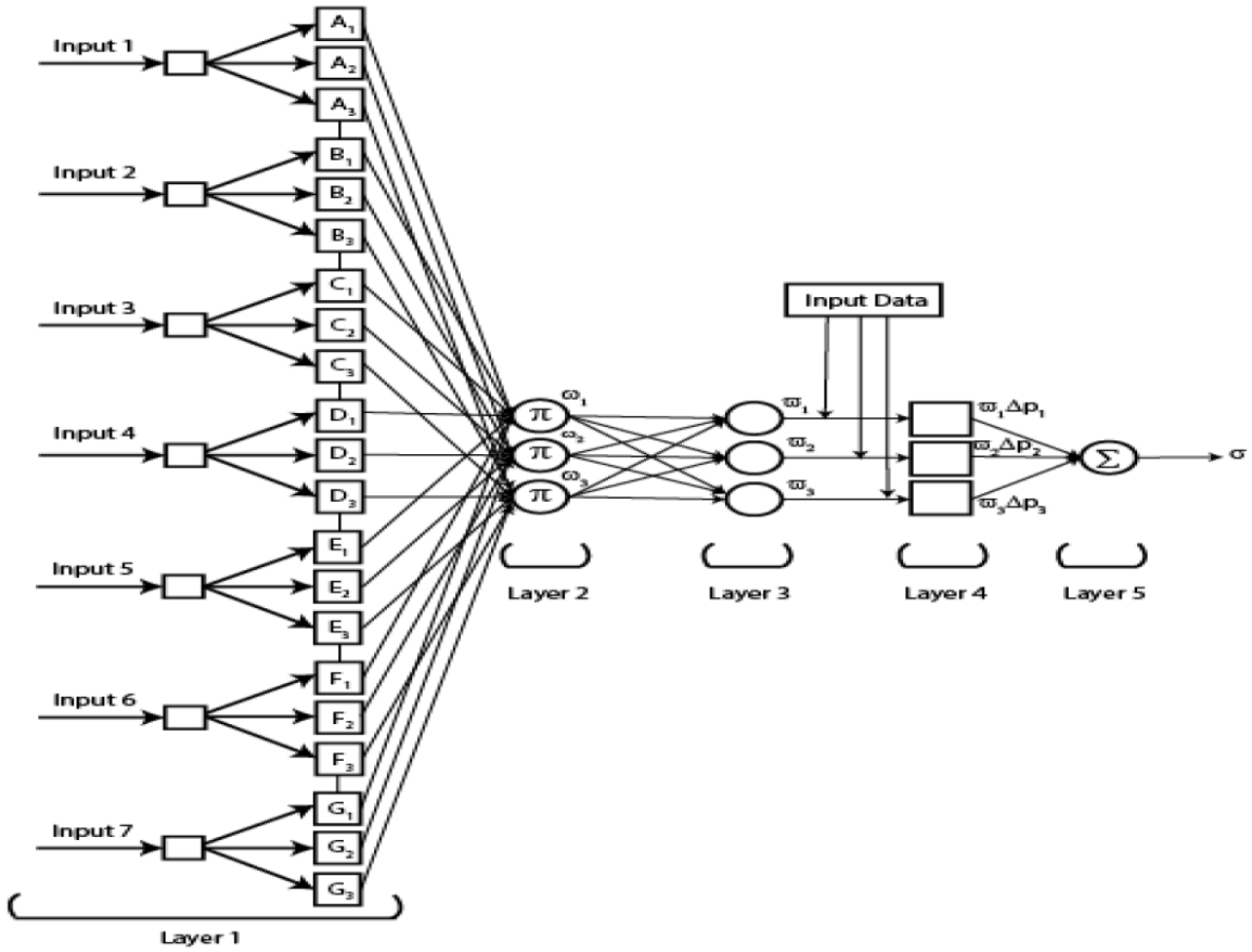

Figure 6. ANFIS model structure.

$$O_{1,i} = \mu_{F_{i-15}}(x) \text{ for } i = 16, 17, 18 \tag{39}$$

$$O_{1,i} = \mu_{G_{i-18}}(x) \text{ for } i = 19, 20, 21 \tag{40}$$

Here x is the input node i and A_i (or B_{i-3}, C_{i-6}, D_{i-9}, E_{i-12}, F_{i-15}, G_{i-18}) is a linguistic label associated with this node. Therefore $O_{1,i}$ is the membership grade of the fuzzy set (A_1, A_2, A_3, B_1, B_2, B_3, C_1, C_2, C_3, D_1, D_2, D_3, E_1, E_2, E_3, F_1, F_2, F_3, G_1, G_2, and G_3). The generalized bell function given in Eq. (41) is used as the MF. The maximum value of this function is equal to 1, while the minimum value is 0. Negative input values are put into the algorithm after calculation of their absolute values. Three generalized functions are used for one input. γ_i, ϕ_i, and υ_i parameters are referred to as the premise parameters. The premise parameters are updated for each epoch using a backpropagation learning algorithm.

$$\mu_i(x) = \frac{1}{1 + \left|\frac{x-\nu_i}{\gamma_i}\right|^{2\phi_i}} \text{ for } i = 1, 2, 3....21 \tag{41}$$

Initial schemes of the three membership functions for each input are given in Figures 7–10 below.

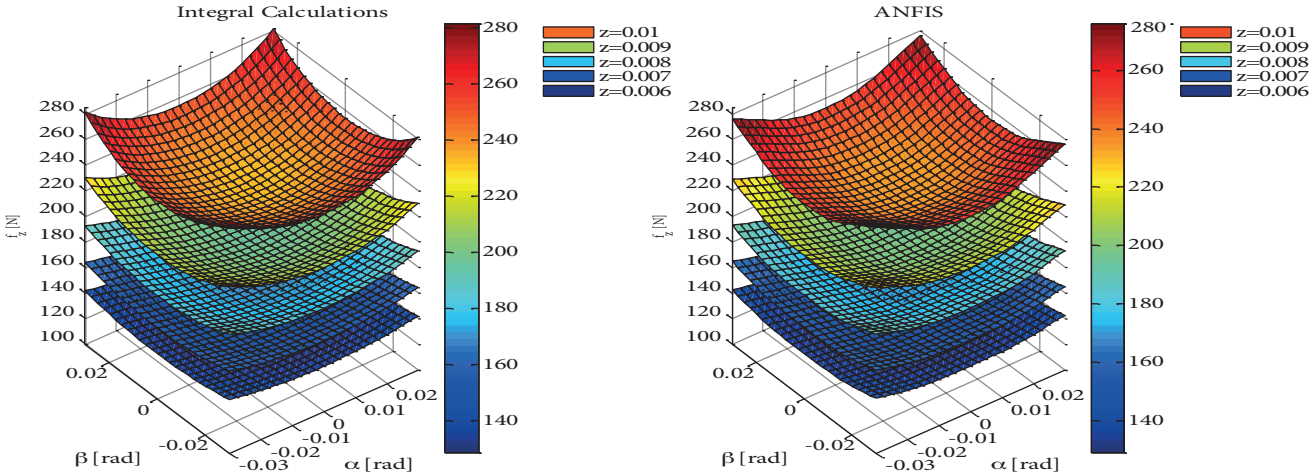

Figure 7. Comparison of integral calculations and ANFIS hybrid learning method.

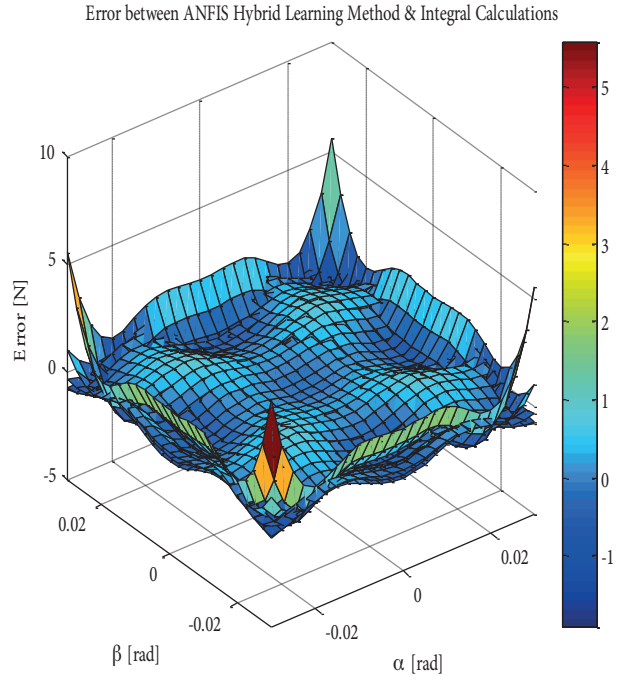

Figure 8. Error between ANFIS method and integral calculations.

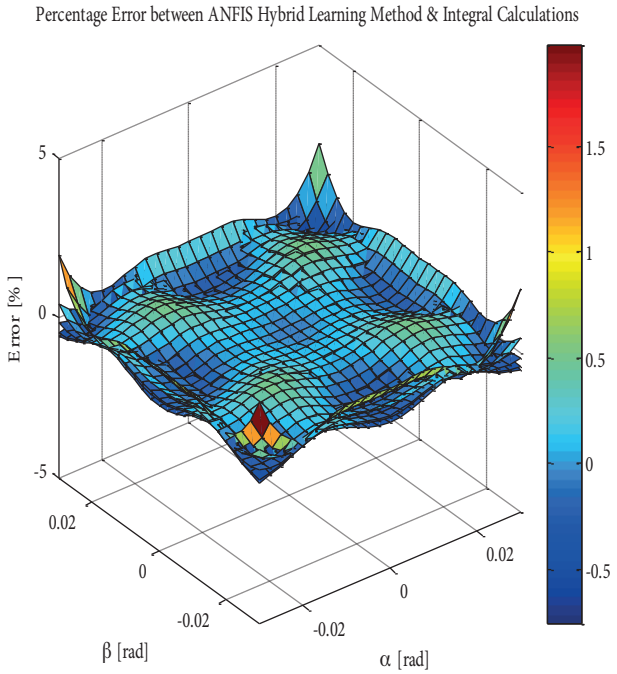

Figure 9. Percentage error between ANFIS method and integral calculations.

In Layer-2, the output is the product of all the incoming signals as given below:

$$O_{2,i} = \omega_i = \mu_{A_i}(x)\mu_{B_i}(x)\mu_{C_i}(x)\mu_{D_i}(x)\mu_{E_i}(x)\mu_{F_i}(x)\mu_{G_i}(x) \quad \text{for} \quad i = 1, 2, 3 \tag{42}$$

In Layer-3, outputs are called normalized firing strengths, given as follows:

$$O_{3,i} = \bar{\omega}_i = \frac{\omega_i}{\omega_1 + \omega_2 + \omega_3} \quad \text{for} \quad i = 1, 2, 3 \tag{43}$$

In Layer-4, every node i in this layer is an adaptive node with a node function given as follows:

$$O_{4,i} = \bar{\omega}_i \Delta p_i = \bar{\omega}_i \underbrace{(p_{1,i}x_A + p_{2,i}x_B + p_{3,i}x_C + p_{4,i}x_D + p_{5,i}x_E + p_{6,i}x_F + p_{7,i}x_G + r_i)}_{\Delta p_i} \text{ for } i = 1,2,3 \quad (44)$$

$p_{1,i}$, $p_{2,i}$, $p_{3,i}$, $p_{4,i}$, $p_{5,i}$, $p_{6,i}$, $p_{7,i}$, and r_i parameters are the consequent parameters and are updated in each epoch by least-squares learning algorithm. Each consequent parameter's initial value is chosen to be 1 in this study.

In Layer-5, this single node in this layer is a fixed node, which computes the overall output as the summation of all incoming signals.

$$O_{5,i} = \sum_i \bar{\omega}_i f_i = \frac{\sum_i \omega_i f_i}{\sum_i \omega_i} \text{ for } i = 1,2,3 \quad (45)$$

In the hybrid learning algorithm, there are two different learning directions. The first learning direction is forward pass using the least-squares method. The second learning direction is backward pass using the backpropagation method.

4. The least-squares method in the hybrid learning algorithm

An adaptive network can be modeled as follows: the system has only one output represented by

$$\sigma = F(\tau, \xi), \quad (46)$$

where τ is the vector of input variables, ξ is the set of parameters, and σ is the overall function implemented by the adaptive network. If there exists a function ψ such that the composite function $\psi\sigma$ is linear in some of the elements of ξ, then these elements can be identified by the least-squares method. To define deeply, when the parameter set ξ is divided into two sets, ξ_1 represents premise parameters and ξ_2 represents consequent parameters.

$$\xi = \xi_1 + \xi_2 \quad (47)$$

such that $\psi\sigma$ is linear in the elements of ξ_2; then upon applying ψ to Eq. (46), Eq. (48) is obtained as follows:

$$\Delta = \psi\kappa\sigma, \quad (48)$$

which is linear in the elements of ξ_2. Now, given initial values of ξ_1, the training data $H(\alpha, \beta, z, I_1, I_2, I_3, I_4)$ can be implemented into Eq. (48), and thus Equation (49) is obtained.

$$A\theta = \lambda, \quad (49)$$

where θ is an unknown vector whose elements are parameters in ξ_2. The least-squares estimator for θ is given below:

$$\theta^* = (A^T A)^{-1} A^T \lambda, \quad (50)$$

where A^T is the transpose of A and $(A^T A)^{-1} A^T$ is the pseudoinverse of A if $A^T A$ is nonsingular.

5. The backpropagation method in the hybrid learning algorithm

For a given training data set H, the error measure for the i_{th} entry can be calculated as the sum of squared errors:

$$E_i = \sum_{k=1}^{N(L)} (d_k - \vartheta_{L,k})^2, \tag{51}$$

where d_k is the k_{th} component of the i_{th} desired output vector and $\vartheta_{L,k}$ is the k_{th} component of the actual output vector produced by presenting the i_{th} input vector to the adaptive network. When E_i is equal to 0, the adaptive network becomes able to produce the exact desired output vector in the i_{th} training data pair, which means the task here is to minimize the error measure.

To create the error signal,

$$\varepsilon_{l,i} = \frac{\partial^+ E_i}{\partial \vartheta_{l,i}} \tag{52}$$

$$\varepsilon_{l,i} = \sum_{m=1}^{N(l+1)} \frac{\partial^+ E_i}{\partial \vartheta_{l+1,m}} \frac{\partial f_{l+1,m}}{\partial \vartheta_{l,i}} \tag{53}$$

$$\frac{\partial^+ E_i}{\partial \omega} = \frac{\partial^+ E_i}{\partial \vartheta_{l,i}} \frac{\partial f_{l,i}}{\partial \omega} = \varepsilon_{l,i} \frac{\partial f_{l,i}}{\partial \omega} \tag{54}$$

The update equation is given below. η is the learning rate and chosen as 0.2 in this study.

$$\Delta\omega = -\eta \frac{\partial^+ E_i}{\partial \omega} \tag{55}$$

6. Results and discussion

6.1. Results for the permanent magnet part of the hybrid electromagnet

In Figure 7, f_z, α, and β correlation results in the case of $I_1 = I_2 = I_3 = I_4 = 0$ are given. In this case, the only working part of the hybrid magnet is the permanent magnet part and torque values do not exist. The leaf on top represents α and β distribution for $z = 0.01$ m, the leaf on the bottom represents α and β distribution for $z = 0.006$ m, and leaves between them are for $z = 0.007$, $z = 0.008$, and $z = 0.009$, respectively. Compared with the ones obtained using multiple integral calculations, it can be said that the ANFIS hybrid learning algorithm shows almost the same behavior pattern. In other words, the designed ANFIS structure is able to mimic the actual 4-pole hybrid electromagnet's behavior for both cases.

To emphasize the success of the proposed method, the error values of the results between the ANFIS hybrid learning algorithm method and multiple integral calculations are given in Figure 8 below. The error values are comparatively acceptable, except the error values occurring on boundary values of training parameters, α and β. Indeed, this situation is expected and usual because the ANFIS hybrid learning algorithm changes its premise and consequent parameters while different parts of the training data are being used in the algorithm. Maximum error, which is 5.4 N, occurs for $z = 0.01$ m. The other leaves give lower maximum error values on the boundaries. Minimum error values mostly occur in the middle of the leaves, which makes sense, because the algorithm runs for the maximum amount of training data around this zone.

To have a look from a different perspective, the percentage error values of the results between the ANFIS hybrid learning algorithm method and multiple integral calculations are given in Figure 9 below. The maximum

percentage error is 1.7%, occurring for $z = 0.01$ m, and the maximum percentage error value for each leaf occurs around the boundaries. The minimum percentage error values mostly occur in the middle of the leaves.

6.2. Results for hybrid electromagnet

In Figures 10–14 below, the correlation between E_α (error between ANFIS method and integral calculations), I_α, and α is given for different z values. For each z value, the minimum error value equals 0. The lowest maximum error value among all z combinations exists for $z = 0.006$, equal to 0.0062. The highest maximum error value exists for $z = 0.008$ m, equal to 0.04 Nm.

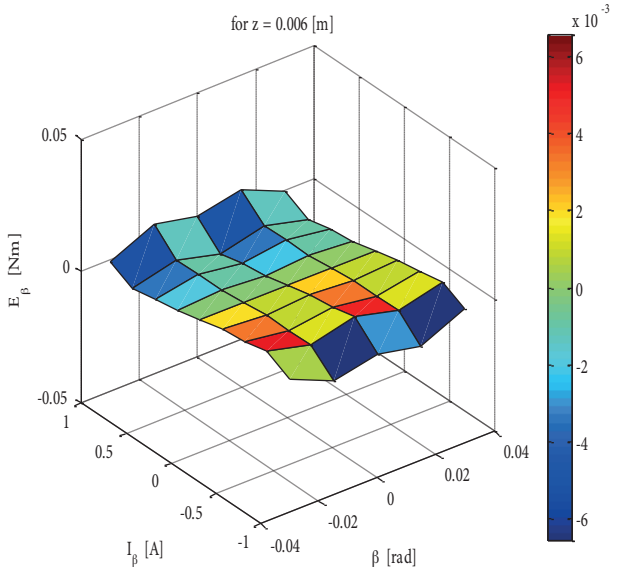

Figure 10. E_α, I_α, and α for z = 0.006 [m].

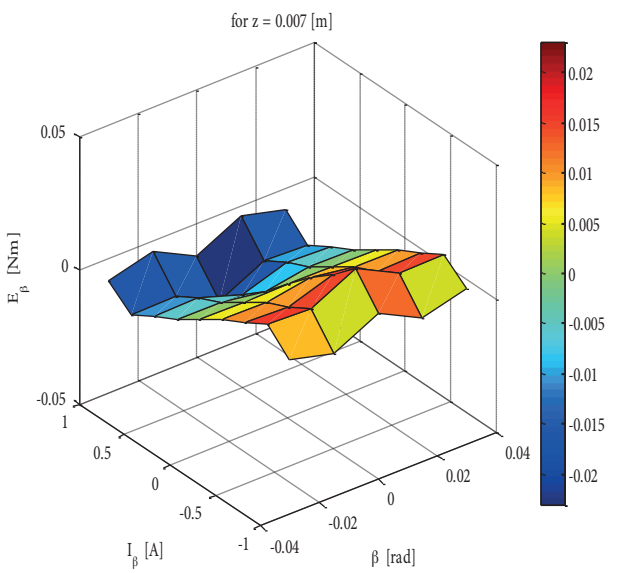

Figure 11. E_α, I_α, and α for z = 0.007 [m].

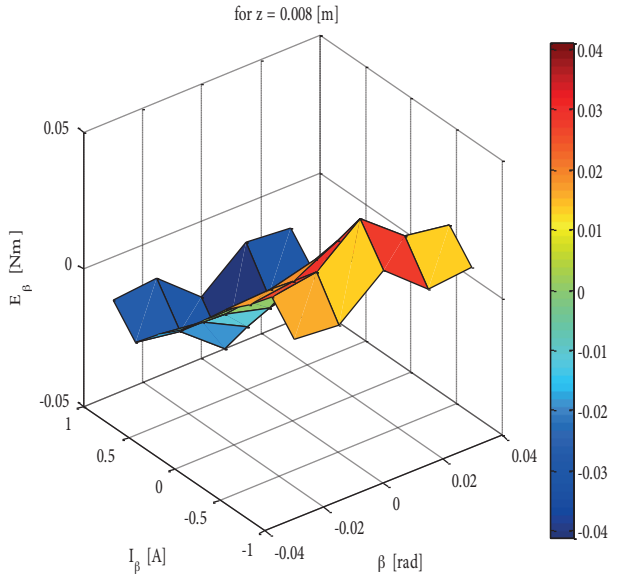

Figure 12. E_α, I_α, and α for z = 0.008 [m].

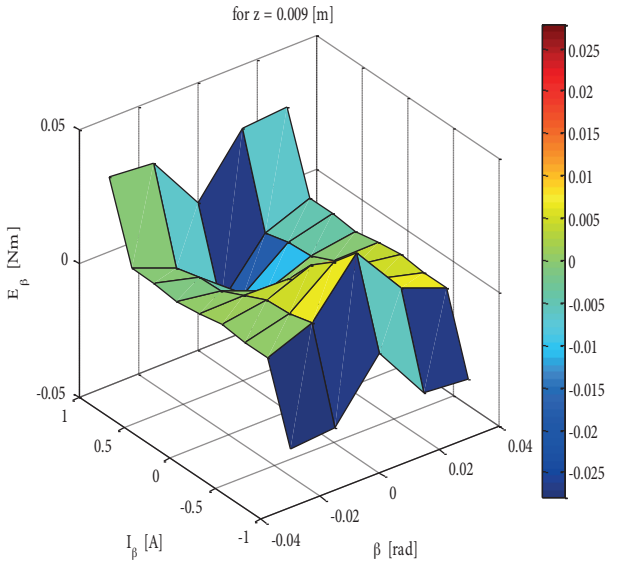

Figure 13. E_α, I_α, and α for z = 0.009 [m].

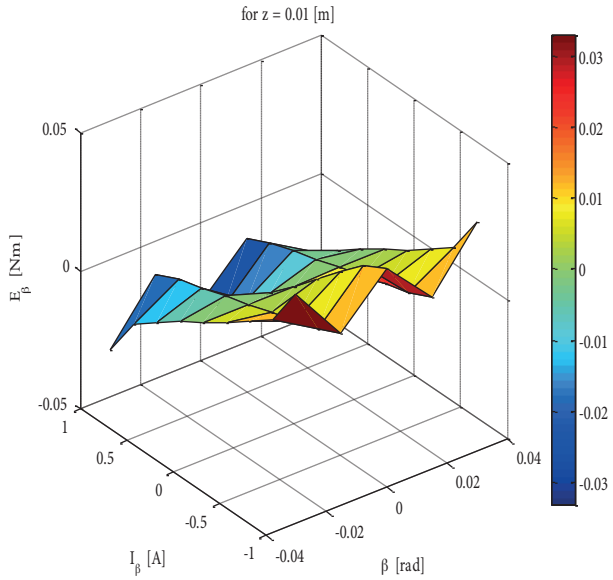

Figure 14. E_α, I_α, and α for z = 0.01 [m].

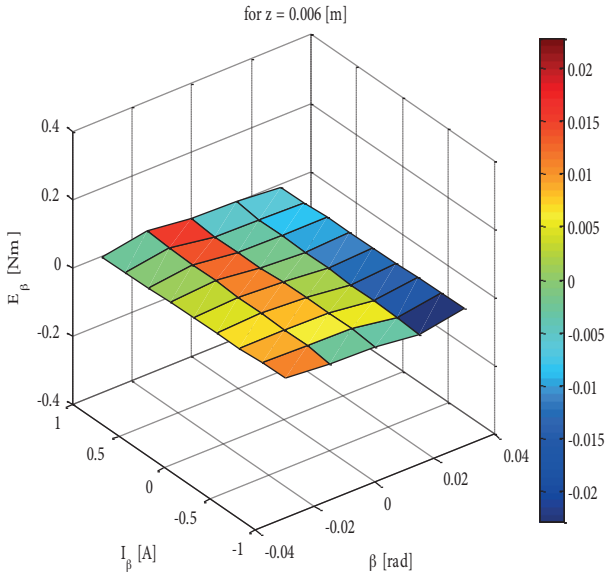

Figure 15. E_β, I_β, and β for z = 0.006 [m].

In Figures 15–19 below, the correlation between E_β (error between ANFIS method and integral calculations), I_β, and β is given for different z values. For each z value, the minimum error value equals 0. The lowest maximum error value among all z combinations exists for $z = 0.006$, equal to 0.021. The highest maximum error value exists for $z = 0.009$ m, equal to 0.31 Nm.

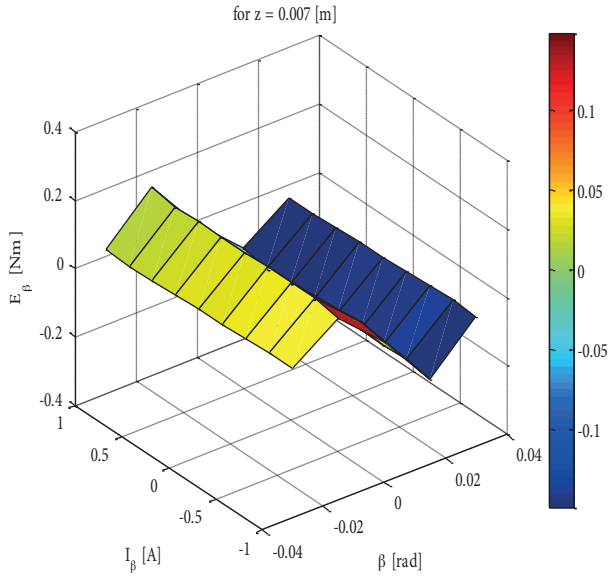

Figure 16. E_β, I_β, and β for z = 0.007 [m].

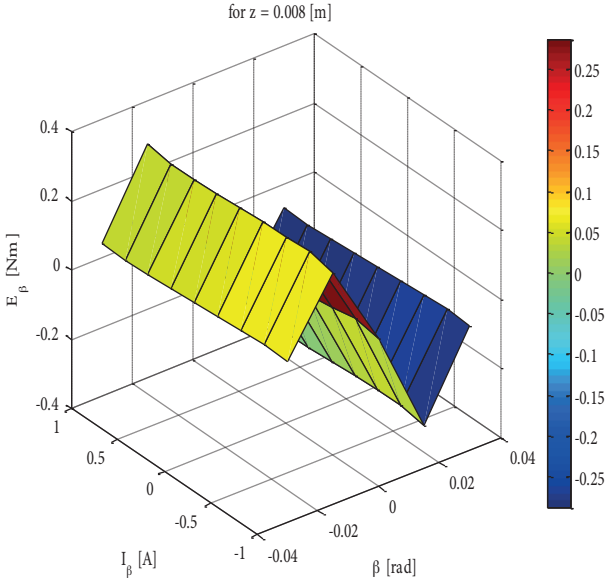

Figure 17. E_β, I_β, and β for z = 0.008 [m].

7. Conclusion

The ANFIS hybrid learning algorithm is successfully capable with the estimation of a 4-pole hybrid electromagnet's force and torque parameters. It is obvious that an expert system acting like a "*look-up table*" for the occurring force and torque values of a 4-pole hybrid electromagnet can be created using this method in some

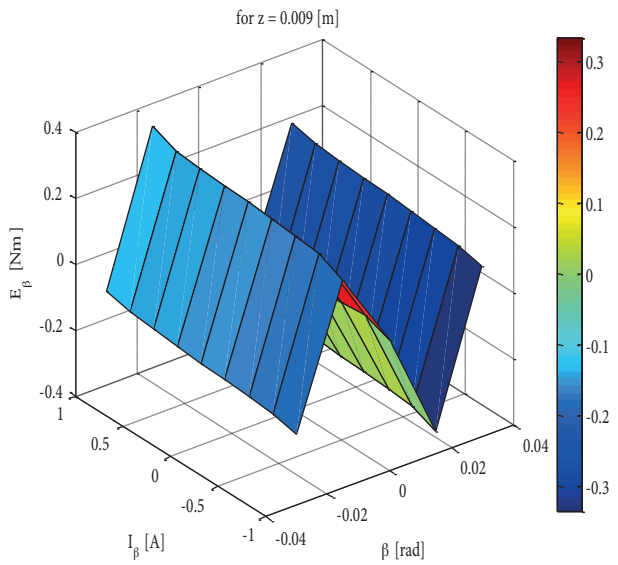

Figure 18. E_β, I_β, and β for z = 0.009 [m].

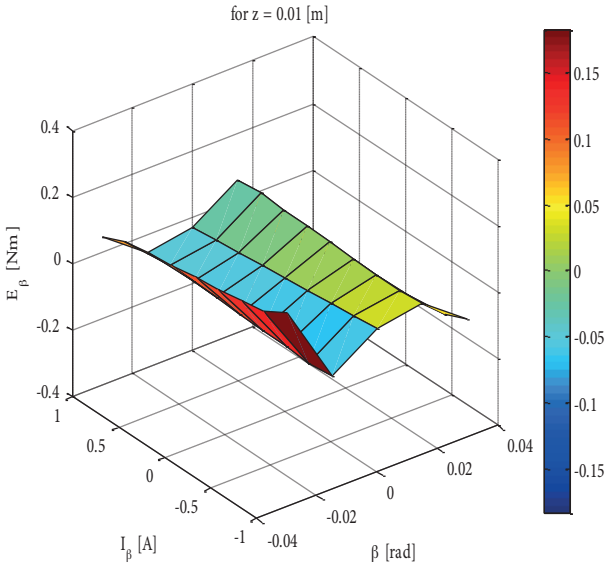

Figure 19. E_β, I_β, and β for z = 0.01 [m].

specific ranges. Moreover, this method cannot only remove the requirement of using high cost data acquisition cards, but also reduce the power consumption due to high sampling rate sensor needs. Another advantage is that, for very complex control algorithms, this method can be used with high cost equipment as a hybrid design, consisting of both estimation and real-time data acquisition, which means the study results open a way to create new advanced control algorithms for magnetic levitation technology.

Acknowledgment

This work was supported by the Scientific and Technological Research Council of Turkey (TÜBİTAK) under the grant number 112M210.

References

[1] Knospe CR. Active magnetic bearings for machining applications. Con Eng Prac 2007; 15: 307-313.

[2] Yang G, Shi Z, Mo N, Zhao L. Research on active magnetic bearing applied in Chinese modular high-temperature gas-cooled reactor. Prog Nuc Eng 2014; 77: 352-360.

[3] Lin FJ, Chen SY, Huang MS. Adaptive complementary sliding-mode control for thrust active magnetic bearing system. Con Eng Prac 2011; 19: 711-722.

[4] Tang J, Sun J, Fang J, Sam GS. Low eddy loss axial hybrid magnetic bearing with gimballing control ability for momentum flywheel. J Mag Mag Mat 2013; 329: 153-164.

[5] Okano M, Iwamoto T, Fuchino S, Tamada N. Feasibility of a goods transportation system with a superconducting magnetic levitation guide – load characteristics of a magnetic levitation guide using a bulk high-Tc superconductor. Phy C: Supercon 2003; 386: 500-505.

[6] D'Ovidio G, Crisi F, Lanzara G. A "V" shaped superconducting levitation module for lift and guidance of a magnetic transportation system. Phy C: Supercon 2008; 468: 1036-1040.

[7] Shu QS, Cheng G, Susta JT, Hull JR, Fesmire JE, Augustanowicz SD, Demko JA, Werfel FN. Magnetic levitation technology and its applications in exploration projects. Cryo 2006; 46: 105-110.

[8] Sari I, Kraft M. A MEMS linear accelerator for levitated micro-objects. Sens Act A: Phy 2015; 222: 15-23.

[9] Kim WJ, Verma S, Shakir H. Design and precision construction of novel magnetic-levitation-based multi-axis nanoscale positioning systems. Pre Eng 2007; 31: 337-350.

[10] van West E, Yamamoto A, Higuchi T. Automatic object release in magnetic and electrostatic levitation systems. Pre Eng 2009; 33: 217-228.

[11] Erkan K, Acarkan B, Koseki T. Zero-power levitation control design for a 4-pole electromagnet on the basis of a transfer function approach. In Elec Mac & D Conf, 2007. IEMDC '07. IEEE Int. 2007.

[12] Bächle T, Hentzelt S, Graichen K. Nonlinear model predictive control of a magnetic levitation system. Con Eng Prac 2013; 21: 1250-1258.

[13] Yang JH, Lee YS, Kwon OK. Development of magnetic force modeling equipment for magnetic levitation system. In Con Auto and Sys (ICCAS), 2010.